

# OPTIMAL INPUT SHAPING FOR VIBRATION CONTROL OF A FLEXIBLE MANIPULATOR USING GENETIC ALGORITHM

<sup>1</sup>Mohammad Amin Rashidifar, <sup>2</sup>Darvish Ahmadi, <sup>3</sup>Ali Amin Rashidifar

<sup>\*1</sup>Islamic Azad University, Shadegan Branch, Shadegan, Iran

<sup>2</sup>Islamic Azad University, Shadegan Branch, Shadegan, Iran

<sup>3</sup>Islamic Azad University, Shadegan Branch, Shadegan, Iran

Email: [rashidifar\\_58@yahoo.com](mailto:rashidifar_58@yahoo.com)

**Abstract** – This article presents optimization of input shaping technique for vibration control of a flexible robot manipulator using genetic algorithms. In this work, a single link flexible robot manipulator that moves in horizontal plane is considered. Modeling is done using Finite Element method where the system is divided into 10 elements and the damping ratio of the system are deduced as 0.026, 0.038 and 0.040 for the first three vibration mode respectively. The input shaping technique is used to reduce vibrations in the system. This method requires estimated values of natural frequencies and damping ratios to generate impulse sequences. It is noted that the input shaping control technique is a better control technique compared to the bang-bang torque input control technique. It can be further optimized by using GA, by determining the optimal natural frequencies to cancel the resonance modes in the system and thus reducing the vibrations. For input shaping with genetic algorithm (ISGA) versus bang-bang (BB) and ISGA versus input shaping, the percentages of vibration improvement in term of area representation is about 2720.03% and 28.57% respectively. In this work, GA optimization method not only reduces the vibrations, but also reduces time delay.

**Keywords** – Genetic Algorithm; vibration control; tracking control; optimization; input shape.

## 1. Introduction

Most existing robotic manipulators are designed and built in a manner to maximize stiffness, in an attempt to minimize system vibration and achieve good positional accuracy (Mohamed and Tokhi, 2004). High stiffness is achieved by using heavy material. As a consequence, such robots are usually heavy with respect to the operating payload. This, in turn, limits the operation speed of the robot manipulation, increases the actuator size, and boosts energy consumption and increase the overall cost. Moreover, the payload to robot weight ratio, under such situation, is low. In order to solve these problems, robotic systems are designed to be lightweight and thus possess some level of flexibility. Conversely, flexible robot manipulator exhibits many advantages over their rigid counterparts: they require less material, are lighter in weight; have higher manipulation speed, lower power consumption, require small actuators, are more maneuverable and transportable, are safer to operate due to reduced inertia, have enhanced back-drive ability due to

elimination of gearing, have less overall cost and higher payload to robot weight ratio (Book and Majette, 1983).

However, the control of flexible robot manipulators to maintain accurate positioning is an extremely challenging problem. Due to the flexible nature and distributed characteristic of the system, the dynamics are highly non-linear and complex. Problems arise due to precise positioning requirement, vibration due to system flexibility, the difficulty in obtaining accurate model of the system and nonminimum phase characteristics of the system (Piedboeuf et al, 1983; Yurkovich, 1992). Therefore, flexible manipulators have not been favored in production industries, as the manipulator is required to have reasonable end-point accuracy in response to input commands. In this respect, a control mechanism that accounts for both rigid body and flexural motions of the system is required. If the advantages associated with lightness are not to be sacrificed, accurate models and efficient controllers have to be developed (Mohamed, Tokhi, 2004).

## 2. The Flexible Manipulator System

A description of the single-link flexible manipulator system considered in this work is shown in Figure 1, where **XY** and **POQ** represents the stationary and moving coordinates frame respectively and  $\tau$  represents the applied torque at the hub.  $E, l, \rho, A, I_h$

And  $M_p$  represents Young modulus, area moment of inertia, mass density per unit volume, cross-sectional area, hub inertia and payload mass of the manipulator respectively. In this work, the motion of the manipulator is confined to the **XY** plane. Since the manipulator is long and slender, transverse shear and rotary inertia effects are neglected. This allows the use of the Bernoulli–Euler beam theory to model the elastic behavior of the manipulator. The manipulator is assumed to be stiff in vertical bending and torsion, allowing it to vibrate dominantly in the horizontal direction thus, the gravity effects is neglected. Moreover, the manipulator is considered to have constant cross-section and uniform material properties throughout. In this study, an aluminum type flexible manipulator of dimensions  $900 \times 19.008 \times 3.2004mm^3$  and  $E = 71 \times 10^9 N/m^2$  and  $I = 5.1924m^4$  and  $\rho = 2710kg/m^3$  is considered.

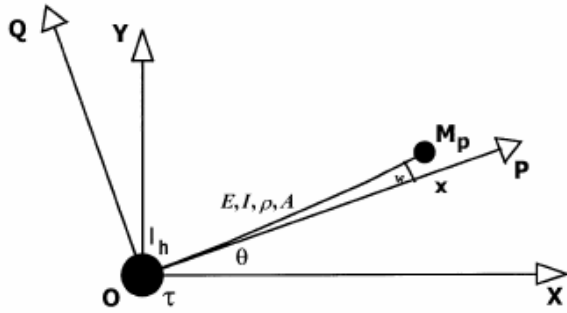


Figure1. Description of the manipulator system.

### 3. Modeling of the Flexible Manipulator

This section briefly describes modeling of the flexible robot manipulator system, as basis of a simulation environment for the development of feed-forward control strategies for vibration control of the system. In this investigation, the FE method with 10 elements is considered in characterizing the dynamic behavior of the manipulator incorporating structural damping and hub inertia. The equations of motion are expressed in state-space form. Simulation results of the dynamic behavior of the manipulator are presented in the time and frequency domains.

For a small angular displacement  $\theta(t)$  and a small elastic deflection  $w(x, t)$ , the total displacement  $y(x, t)$  of a point along the manipulator at a distance  $x$  from the hub can be described as a function of both the rigid body motion  $\theta(t)$  and elastic deflection  $y(x, t)$  measured from the line  $OX$  as:

$$y(x, t) = x\theta(t) + w(x, t) \quad (1)$$

Using the FE method, kinetic and potential energies of an element, yields the element mass matrix,  $M_n$  and stiffness matrix  $K_n$  as:

$$M_n = \frac{\rho Al}{420} \begin{bmatrix} m_{11} & m_{12} & m_{13} & m_{14} & m_{15} \\ m_{21} & 156 & 22l & 54 & -13l \\ m_{31} & 22l & 4l^2 & -13l & -3l^2 \\ m_{41} & 54 & -13l & 156 & 22l \\ m_{51} & -13l & -3l^2 & 22l & 4l^2 \end{bmatrix} \quad (2)$$

$$K_n = \frac{EI}{l^3} \begin{bmatrix} 0 & 0 & 0 & 0 & 0 \\ 0 & 12 & -6l & -12 & 6l \\ 0 & 6l & 4l^2 & -6l & 2l^2 \\ 0 & -12 & -6l & 12 & 6l \\ 0 & 6l & 2l^2 & -6l & 4l^2 \end{bmatrix} \quad (3)$$

Where

$$\begin{aligned} m_{11} &= 140l^2(3n^2 - 3n + 1) \\ m_{12} &= m_{21} = 21l(10n - 7) \\ m_{13} &= m_{31} = 7l^2(5n - 3) \\ m_{14} &= m_{41} = 21l(10n - 3) \\ m_{15} &= m_{51} = -7l^2(5n - 3) \end{aligned}$$

That  $l$  is the elemental length of the manipulator and  $n$  is the number of elements.

Assembling the element mass and stiffness matrices by utilizing the Lagrange equation of motion, the desired dynamic equations of motion of the system can be obtained as:

$$M\ddot{Q}(t) + D\dot{Q}(t) + KQ = F(t) \quad (4)$$

Where  $M, D$  and  $K$  are global mass, damping and stiffness matrices of the manipulator respectively. The damping matrix is obtained by assuming that the manipulator exhibits the characteristics of Rayleigh damping.  $F(t)$  is a vector of external forces.  $Q(t)$  is a nodal displacement vector given as:

$$Q(t) = [\theta \ w_0 \ \dots \ w_n \ \theta_n]^T \quad (5)$$

Where  $w_n(t)$  and  $\theta_n(t)$  are the flexural and angular deflections at the end point of the manipulator respectively. With 10 elements, the  $M, D$  and  $K$  matrices in Equation 4 are of size  $m \times m$  and  $F(t)$  is of size  $m \times 1$ , where  $m = 21$ . For the manipulator, considered as a pinned-free arm with the applied torque  $\tau$  at the hub, the flexural and angular deflections, velocity and acceleration are all zero at the hub at  $\tau$  and the external force is

$$F(t) = [\tau \ 0 \ \dots \ 0]^T$$

Moreover, in this work, it is assumed that  $Q(0) = 0$ . The matrix differential equation in Equation 4 can be represented in a state space form as:

$$\begin{aligned} \dot{v} &= Av + Bu \\ y &= Cv \end{aligned} \quad (6)$$

Where

$$A = \begin{bmatrix} 0_m & I_m \\ -M^{-1}K & -M^{-1}D \end{bmatrix}, B = \begin{bmatrix} 0_{m \times 1} \\ M^{-1} \end{bmatrix}, C = [I_{2m}] \quad (7)$$

And

$$u = [\tau \ 0 \ \dots \ 0] \quad (8)$$

$$v = [\theta \ w_1 \ \theta_1 \ \dots \ w_n \ \theta_n \ \dot{\theta} \ \dot{w}_1 \ \dot{\theta}_1 \ \dots \ \dot{w}_n \ \dot{\theta}_n]^T$$

Solving the state-space matrices gives the vector of states  $v$ , that is, the angular, nodal flexural and angular displacements, and velocities.

To assess the adequacy of the FE model, simulation results of the dynamic behavior of the flexible manipulator using 10 elements are presented in time and frequency domains. Previous experimental study on the actual flexible manipulator has shown that the damping ratio of the system ranges from 0.024 to 0.1.

In this work, the damping ratios of the system were deduced as 0.026, 0.038 and 0.04 for the first, second and third modes respectively. Figure 3.2 shows a single switch bang–bang signal of amplitude 0.3 Nm used as an input torque, applied at the hub of the manipulator.

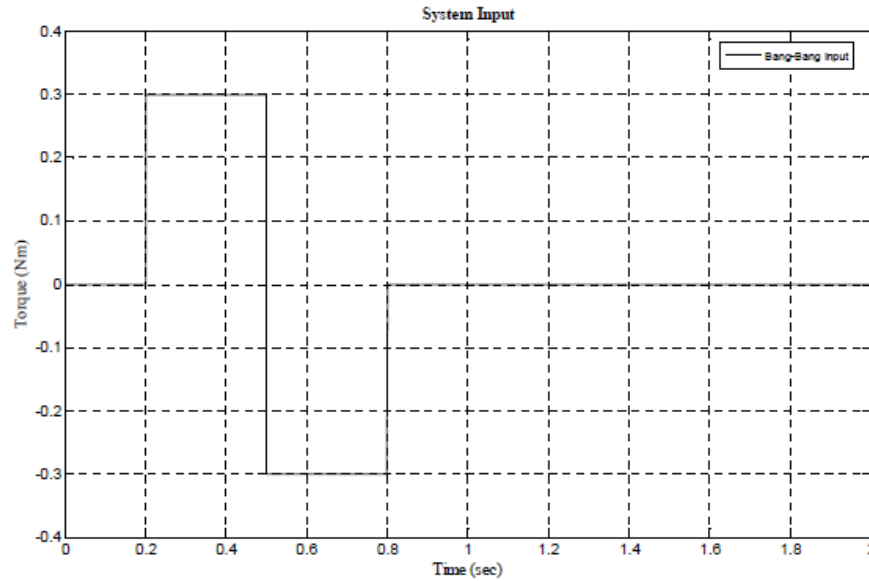


Figure2. The bang-bang input.

A bang–bang torque has a positive (acceleration) and negative (deceleration) period allowing the manipulator to, initially, accelerate and then decelerate and eventually stop at a target location. Four system responses namely end-point displacement, hub-angle, hub-velocity and end-point

residual and its SD are obtained. The results are recorded with a sampling frequency of 2 kHz as shown in Figure 3. In this work, the first three modes of vibration are considered, as this dominantly characterizes the behavior of the flexible manipulator.

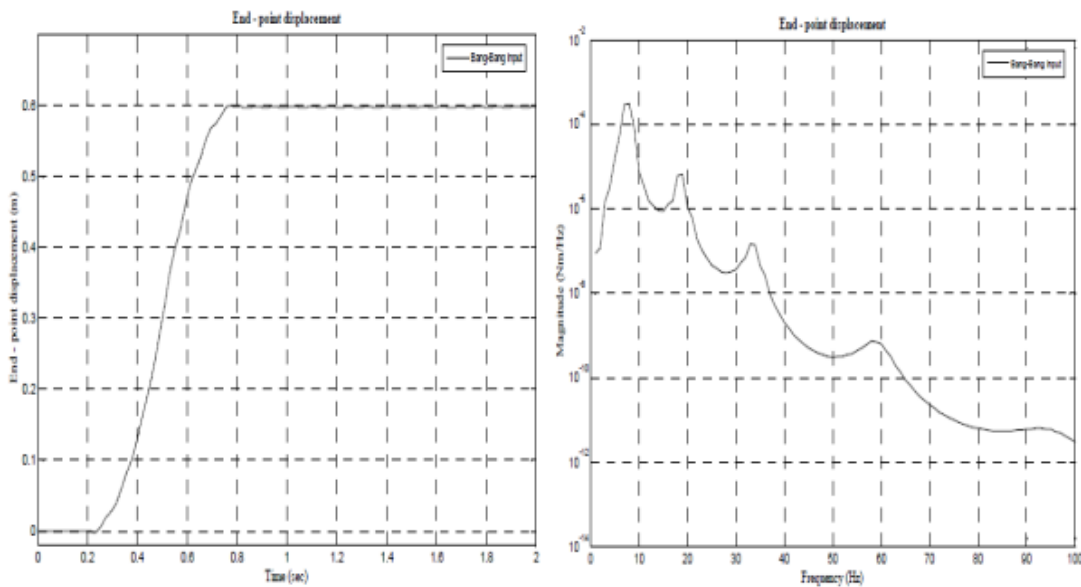


Figure3. Response of the flexible manipulator to the bang-bang torque input. a) End point displacement. b) SD of end-point displacement.

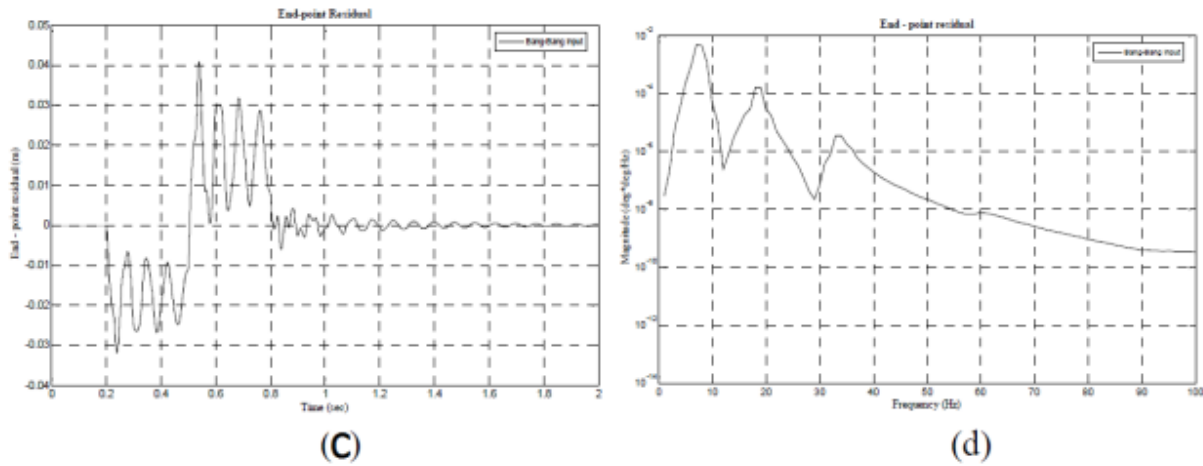


Figure4. Response of the flexible manipulator to the bang-bang torque input. c) End-point residual d) SD of end-point residual.

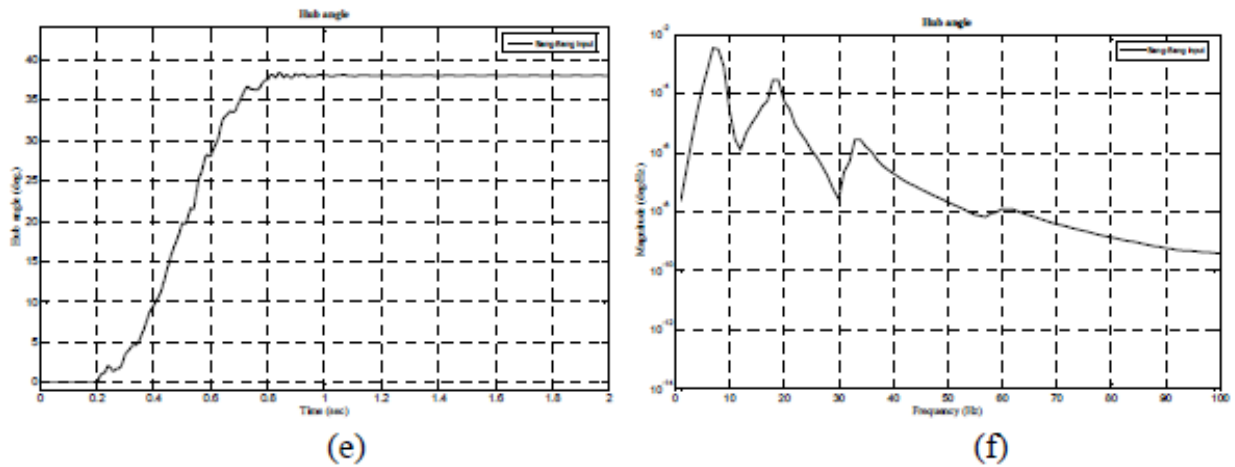


Figure5. Response of the flexible manipulator to the bang-bang torque input. e) Hub angle. f) SD of hub angle.

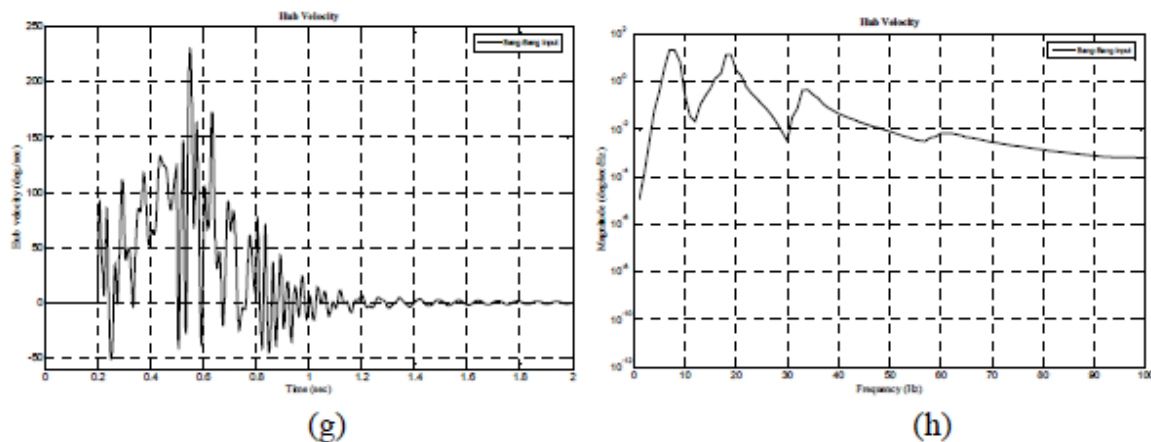


Figure5. Response of the flexible manipulator to the bang-bang torque input. g) Hub velocity h) SD of hub velocity.

#### 4. Input Shaping

The input shaping method involves convolving a desired command with a sequence of impulses. The design

objectives are to determine the amplitude and time location of the impulses. A vibratory system of any order can be modeled as superposition of second order systems with a transfer functions:

$$G(s) = \frac{\omega^2}{s^2 + 2\xi\omega s + \omega^2} \quad (9)$$

Where  $\omega$  is the natural frequency and  $\xi$  is the damping ratio of the system. Thus, the impulse response of the system can be obtained as:

$$y(t) = \frac{A\omega}{\sqrt{1-\xi^2}} e^{-\xi\omega(t-t_0)} \sin(\omega\sqrt{1-\xi^2}(t-t_0)) \quad (10)$$

Where  $A$  and  $t_0$  are the amplitudes and the time of impulse respectively. Furthermore, the response to a sequence of impulse can be obtained by superposition of the impulse response. Thus, for  $N$  impulse, with  $\omega_d = \omega(\sqrt{1-\xi^2})$ , the impulse response can be expressed as:

$$y(t) = M \sin(\omega_d t + \beta) \quad (11)$$

Where

$$M = \sqrt{(\sum_{i=1}^N B_i \cos \varphi_i)^2 + (\sum_{i=1}^N B_i \sin \varphi_i)^2} \quad (12)$$

And

$$B_i = \frac{A_i \omega}{\sqrt{1-\xi^2}} e^{-\xi\omega(t-t_0)}, \varphi_i = \omega_d t_i \quad (13)$$

$A_i$  and  $t_i$  are the amplitudes and times of the impulses.

The residual single mode vibration amplitude of the impulse response is obtained at the time of the last impulse,  $t_N$  as:

$$V = V_1^2 + V_2^2 \quad (14)$$

Where

$$V_1 = \sum_{i=1}^N \frac{A_i \omega_n}{\sqrt{1-\xi^2}} e^{-\xi\omega(t_n-t_i)} \cos \omega_d t_i, V_2 = \sum_{i=1}^N \frac{A_i \omega_n}{\sqrt{1-\xi^2}} e^{-\xi\omega(t_n-t_i)} \sin \omega_d t_i \quad (15)$$

To achieve zero vibration after the last impulse, it is required that both  $V_1$  and  $V_2$  in Equation 15 are independently zero. Furthermore, to ensure that the shaped command input produces the same rigid body motion as the unshaped command, it is required that the sum of amplitudes of the impulse is unity. To avoid response delay, the first impulse is selected at time  $t_1 = 0$ . Hence by setting  $V_1$  and  $V_2$  in equation 14 to zero  $\sum_{i=1}^N A_i = 1$  and solving this yield a two-impulse sequence with parameters such as:

$$t_1 = 0, t_2 = \frac{\pi}{\omega_d}, A_1 = \frac{1}{1+K}, A_2 = \frac{K}{1+K} \quad (16)$$

Where

$$K = e^{\frac{\xi\pi}{\sqrt{1-\xi^2}}} \quad (17)$$

The robustness of the input shaper to error in natural frequencies of the system can be increased by setting  $dV/d\omega = 0$ , where  $dV/d\omega$  is the rate of change of  $V$  with respect to  $\omega$ . Setting the derivative to zero is

equivalent of producing small changes in vibration with corresponding changes in the natural frequency. Thus, additional constraints are incorporated into the equation, which after solving, yields three impulse sequences with parameter as:

$$t_1 = 0, t_2 = \frac{\pi}{\omega_d}, t_3 = 2t_2, A_1 = \frac{1}{1+2K+K^2} \\ A_2 = \frac{2K}{1+2K+K^2}, A_3 = \frac{K^2}{1+2K+K^2} \quad (18)$$

where  $K$  is as in Equation 17. The robustness of the input shaper can further be increased by taking and solving the second derivative of the vibration in Equation 15. Similarly, this yields, four-impulse sequences with parameters as:

$$t_1 = 0, t_2 = \frac{\pi}{\omega_d}, t_3 = 2t_2, t_4 = 3t_2 \\ A_1 = \frac{1}{1+3K+3K^2+K^3} \\ A_2 = \frac{3K^2}{1+3K+3K^2+K^3} \\ A_3 = \frac{3K^2}{1+3K+3K^2+K^3} \\ A_4 = \frac{K^3}{1+3K+3K^2+K^3} \quad (19)$$

Where  $K$  is as in Equation 17. To handle higher vibration modes, an impulse sequence for each vibration mode can be designed independently. Then, the impulse sequence can be convolved together to form a sequence of impulses that attenuates vibration at higher modes. For any vibratory system, the vibration reduction can be accomplished by convolving any desired system input with an impulse sequence. This yields a shaped input that drives the system to a location without vibration.

## 5. Optimization Problem

The vibration of the flexible manipulator system is minimized by optimizing the impulse sequence. The vibration of the flexible manipulator is represented as the area under the graph of the absolute value of end point acceleration. Thus, the objective of the optimization is to minimize the absolute area under the graph of end point acceleration. In order to attain this objective, the entire system needs to simulated using random sequence of impulses generated by the GA. Figure 6 shows the objective of optimization.

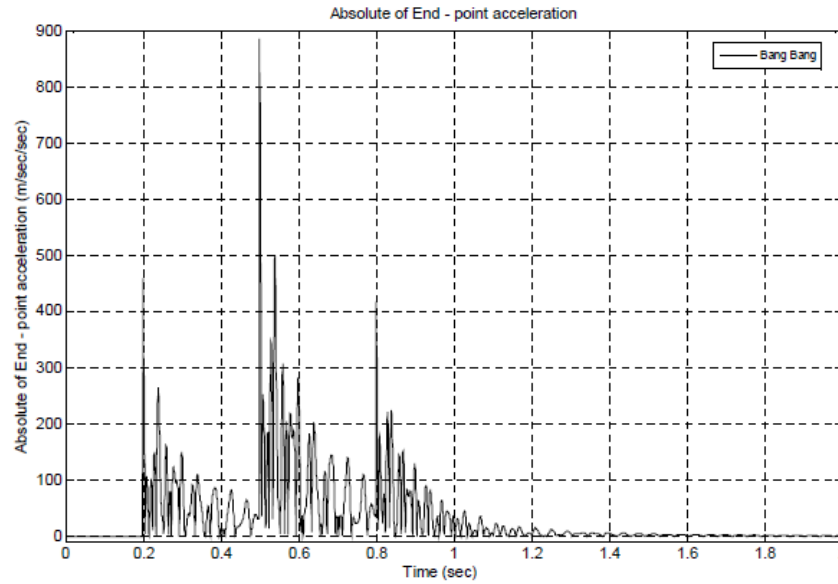


Figure6. The absolute of end-point acceleration

### 7. GA Simulation

A new population is created as a result of completing one iteration of the GA. This procedure can be repeated as many times as desired. In this work, the test run is terminated after 50 generation. This is to force the GA to find optimal result although it has reached the convergence point. The results are obtained as follows:

- Generation 1: (frequency: 12.982910, 37.462577, 59.378347) = 2.683266
- Generation 2: (frequency: 12.982910, 37.462577, 59.378347) = 2.683266
- Generation 3: (frequency: 12.982910, 37.462577, 59.378347) = 2.683266
- Generation 4: (frequency: 12.982910, 37.462577, 59.378347) = 2.683266
- Generation 5: (frequency: 12.982910, 37.462577, 60.423209) = 2.668887
- Generation 6: (frequency: 13.822156, 39.322271, 61.254292) = 2.589630
- Generation 7: (frequency: 13.827039, 39.322271, 61.251545) = 2.566714
- Generation 8: (frequency: 13.827039, 39.322271, 61.251545) = 2.566714
- Generation 9: (frequency: 13.827039, 39.322271, 61.251545) = 2.566714
- Generation 10: (frequency: 13.827039, 39.322271, 61.251545) = 2.566714
- Generation 11: (frequency: 13.827039, 39.322271, 61.251545) = 2.566714
- Generation 12: (frequency: 13.827039, 39.322271, 61.251545) = 2.566714
- Generation 13: (frequency: 13.827039, 39.322271, 61.251545) = 2.566714
- Generation 14: (frequency: 13.827039, 39.791028, 61.192721) = 2.559957
- Generation 15: (frequency: 13.827039, 39.791028, 61.192721) = 2.559957
- Generation 16: (frequency: 13.827039, 39.381094, 64.942779) = 2.536722
- Generation 17: (frequency: 13.827039, 39.381094, 64.942779) = 2.536722
- Generation 18: (frequency: 13.827039, 39.381094, 64.942779) = 2.536722
- Generation 19: (frequency: 13.827039, 39.381094, 64.942779) = 2.536722
- Generation 20: (frequency: 13.827039, 39.381094, 64.942779) = 2.536722

- Generation 21: (frequency: 13.827039, 39.381094, 64.942779) = 2.536722
- Generation 22: (frequency: 13.827039, 39.381094, 64.942779) = 2.536722
- Generation 23: (frequency: 13.827039, 39.381094, 64.942779) = 2.536722
- Generation 24: (frequency: 13.827649, 39.819638, 65.230488) = 2.506673
- Generation 25: (frequency: 13.827649, 39.819638, 65.230488) = 2.506673
- Generation 26: (frequency: 13.827039, 39.789425, 65.872969) = 2.489638
- Generation 27: (frequency: 13.827039, 39.789425, 65.872969) = 2.489638
- Generation 28: (frequency: 13.827039, 39.789425, 65.872969) = 2.489638
- Generation 29: (frequency: 13.827039, 39.789425, 65.872969) = 2.489638
- Generation 30: (frequency: 13.827039, 39.789425, 65.872969) = 2.489638
- Generation 31: (frequency: 13.827039, 39.789425, 65.872969) = 2.489638
- Generation 32: (frequency: 13.827039, 39.789425, 65.872969) = 2.489638
- Generation 33: (frequency: 13.827039, 39.789425, 65.872969) = 2.489638
- Generation 34: (frequency: 13.827039, 39.789425, 65.872969) = 2.489638
- Generation 35: (frequency: 13.827039, 39.789425, 65.872969) = 2.489638
- Generation 36: (frequency: 13.827039, 39.789425, 65.872969) = 2.489638
- Generation 37: (frequency: 13.827039, 39.789425, 65.872969) = 2.489638
- Generation 38: (frequency: 13.827039, 39.789425, 65.872969) = 2.489638
- Generation 39: (frequency: 13.827039, 39.789425, 65.872969) = 2.489638
- Generation 40: (frequency: 13.827039, 39.789425, 65.872969) = 2.489638
- Generation 41: (frequency: 13.827039, 39.789425, 65.872969) = 2.489638
- Generation 42: (frequency: 13.827039, 39.789425, 65.872969) = 2.489638
- Generation 43: (frequency: 13.827039, 39.789425, 65.872969) = 2.489638
- Generation 44: (frequency: 13.827039, 39.789425, 65.872969) = 2.489638
- Generation 45: (frequency: 13.827039, 39.789425, 65.872969) = 2.489638
- Generation 46: (frequency: 13.827039, 39.789425, 65.872969) = 2.489638
- Generation 47: (frequency: 13.827039, 39.789425, 65.872969) = 2.489638
- Generation 48: (frequency: 13.827039, 39.789425, 65.872969) = 2.489638
- Generation 49: (frequency: 13.827039, 39.789425, 65.872969) = 2.489638
- Generation 50: (frequency: 13.827039, 39.789425, 65.872969) = 2.489638

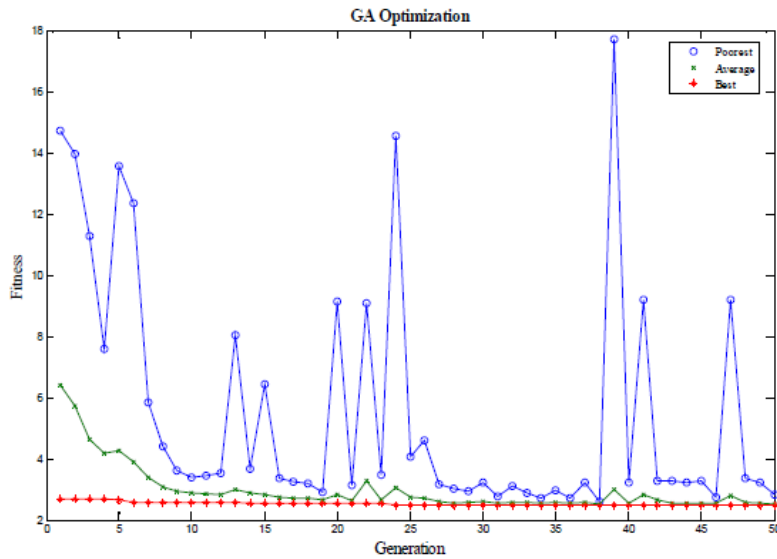


Figure7. The optimization of GA

Figure 7 is a plot of the best, average and poorest values of the objective function across 50 generation. Since reproduction is used to keep the best two individuals at each generation, the “best” curve is monotonically decreasing with the respect to generation numbers and thus, the GA is able to track the minimal point within few generations. The erratic behavior of the ‘poorest’ curve is due to mutation and crossover operator, which explores the landscape in a somewhat random manner. In this work, the GA is forced to iterate 50 generation although the GA has converged and reach the optimal point. This is to shows

that the GA continues to explore the objective function surface although it has reached the optimal point. In GA, random numbers are used, thus there are slight difference in the results of different simulation. Therefore, the same problem is recalculated several time and the results are compared to get an optimal result. Figure 8 illustrates the flow chart of the research methodology. It is very important to define the research methodology as it describes, predicts, select methods, controls, collects data, analyzes and elucidates the way the research has done. This article is illustrated for more understanding.

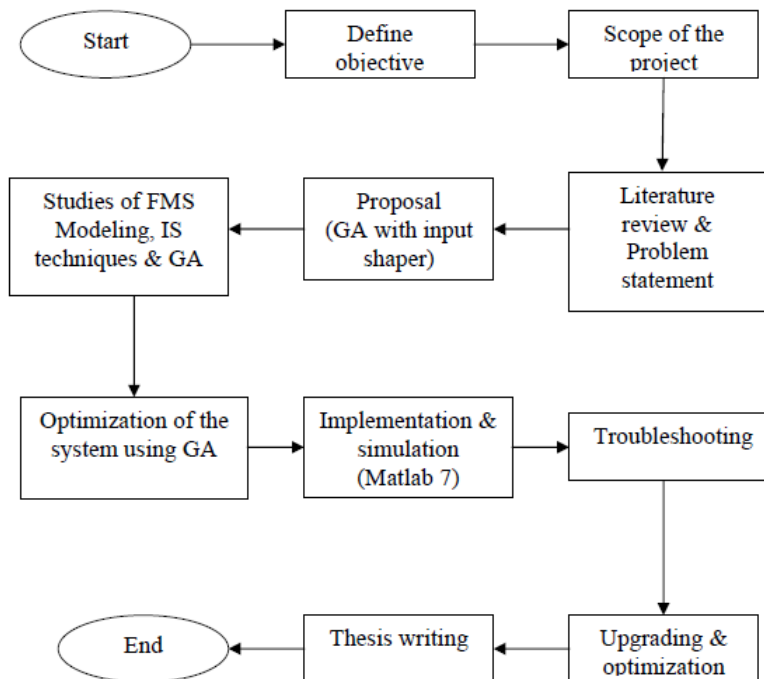


Figure8. Flow chart of search methodology.

### 8. Results

The bang-bang torque input, input shaping and input shaping with GA are compared to verify the performance of the control techniques as shown in Figure 5.3. The simulation can be repeated for different payload of the

system varying from 0 to 100g. In this work, 0g payload is used. The values of natural frequencies obtained from GA simulations are 13.827039 Hz, 39.789425 Hz, and 65.872969 Hz for the first three vibration modes respectively.

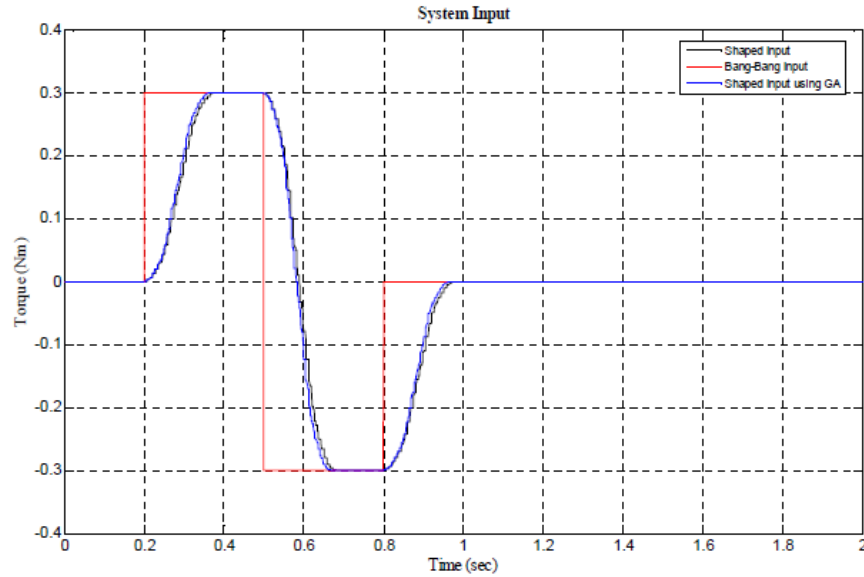


Figure9. The system input

Figure 10 shows the response at the end-point displacement of the flexible manipulator system. The transient response of shaped input control is smoother. Compared to bang-bang torque input control and further optimized using GA for faster response. The steady state response of the shaped input control is better than the bang-bang torque control. The shaped input control performs similar to critically damped and the bang-bang torque

control performs similar to under damped (slight overshoot and oscillation until 2s). The oscillation in bang-bang torque input control delays the system to achieve the desired location accurately. Figure 11 shows that a significant amount of the vibrations are reduced at the resonance modes using ISGA. The characteristic of end-point displacement are compared and as shown as in Table 1.

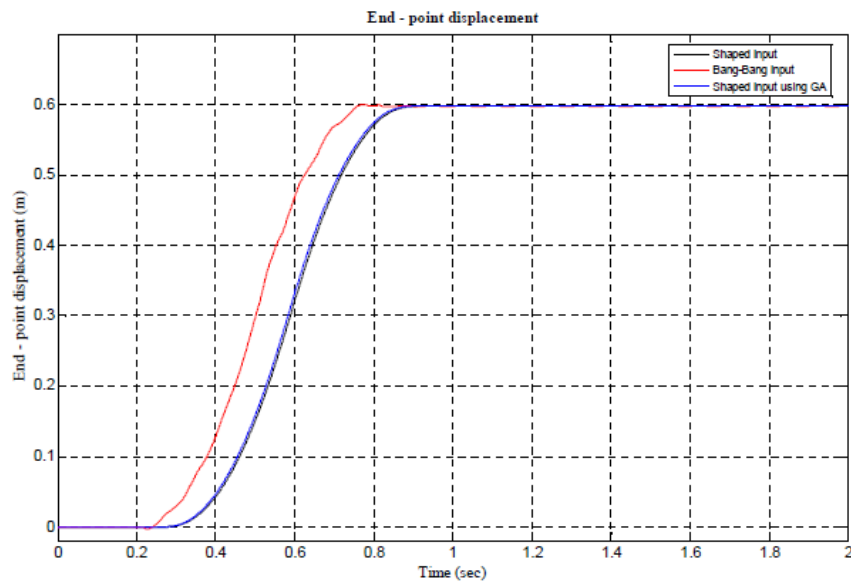


Figure10. End-point displacement (Time domain).

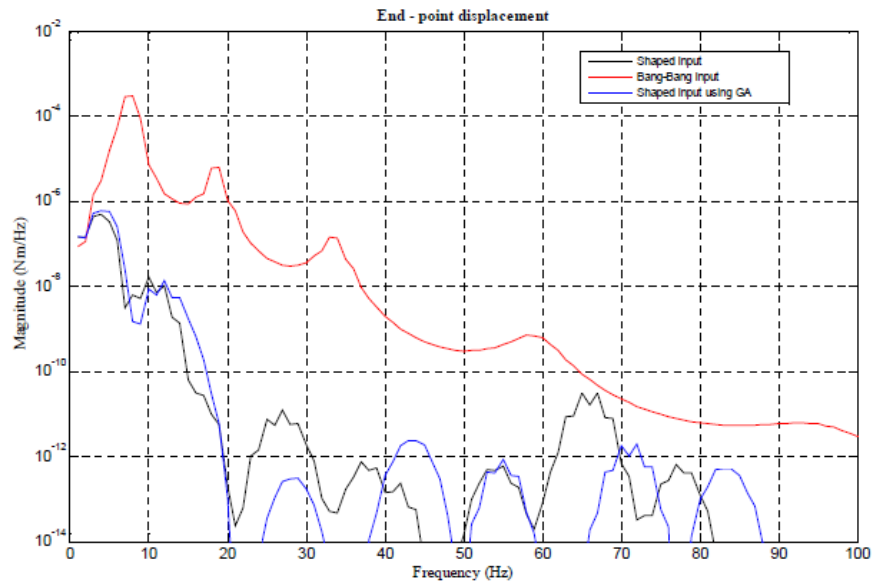


Figure11. End-point displacement (SD of end-point Displacement).

Table1. Characteristic of the system response

Characteristic(sec)	Input Shaping Using Genetic Algorithm (ISGA)	Input Shaping	Bang-Bang torque
Rise time $T_r$	0.334	0.336	0.328
Settling time $T_s$	0.907	0.922	1.8
Time Delay $T_d$	0.02	0.02	-
Time constant T	0.178	0.180	0.171

Figure 12 shows the end-point residual response of the system. It is noted that vibratory response from bang-bang torque input occurs due to resonance modes of the system. The end-point residue response is improved using input shaping technique and further optimized using GA for faster response.

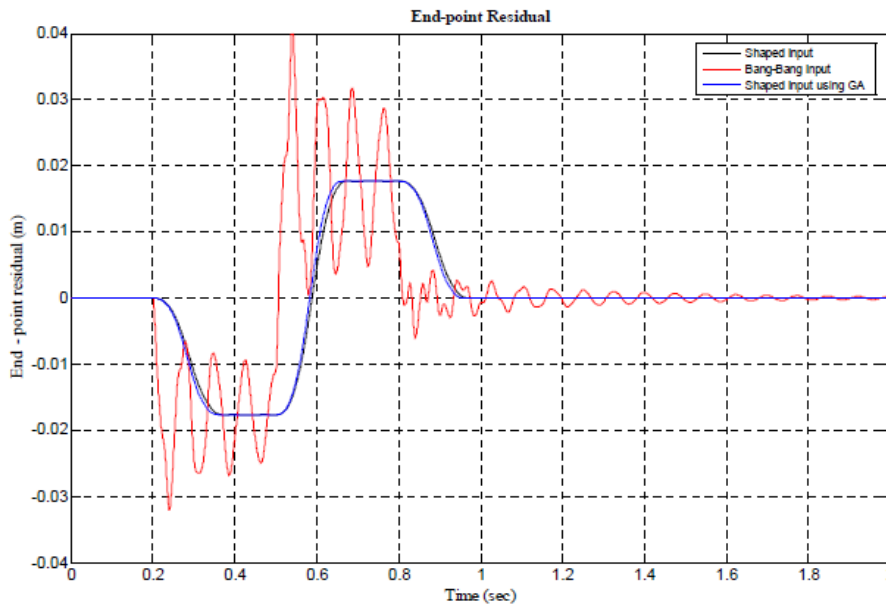


Figure12. End-point residual (Time domain).

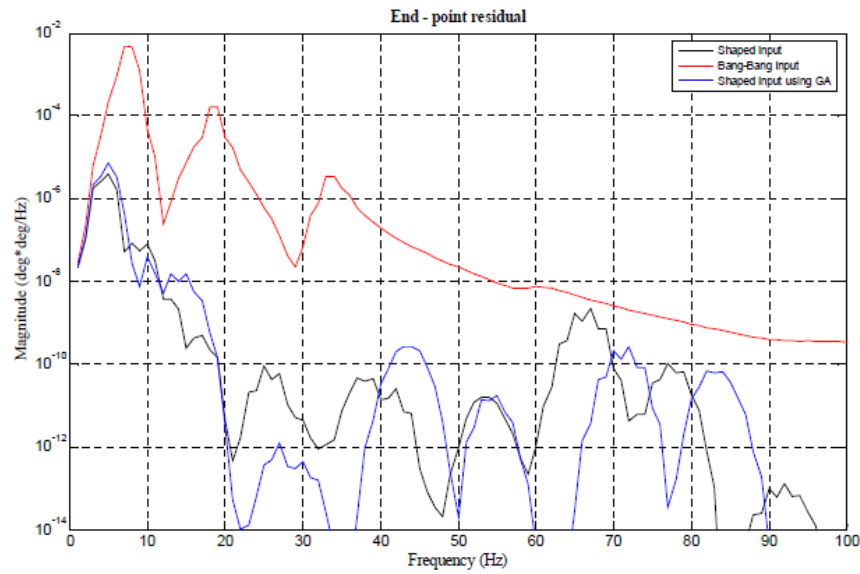


Figure13. End-point residual (SD of end-point residual).

The performance of end-point acceleration is compared in terms of system input and its vibrations and is shown in Table 2.

	Algorithm (ISGA)		
Absolute area	2.48964	3.20081	70.20866
% of vibration improvement in term of area representation comparing ISGA		28.57	2720.03

Table2. The end point acceleration

End-point acceleration	Input Shaping Using Genetic	Input Shaping	Bang-Bang torque
------------------------	-----------------------------	---------------	------------------

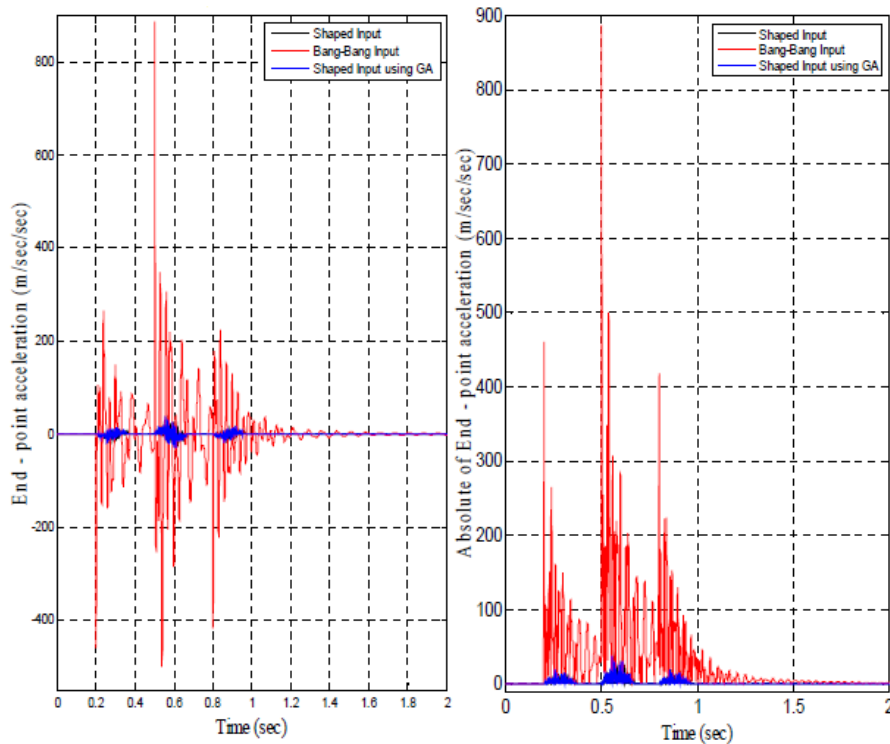


Figure13. End point acceleration (Time domain).

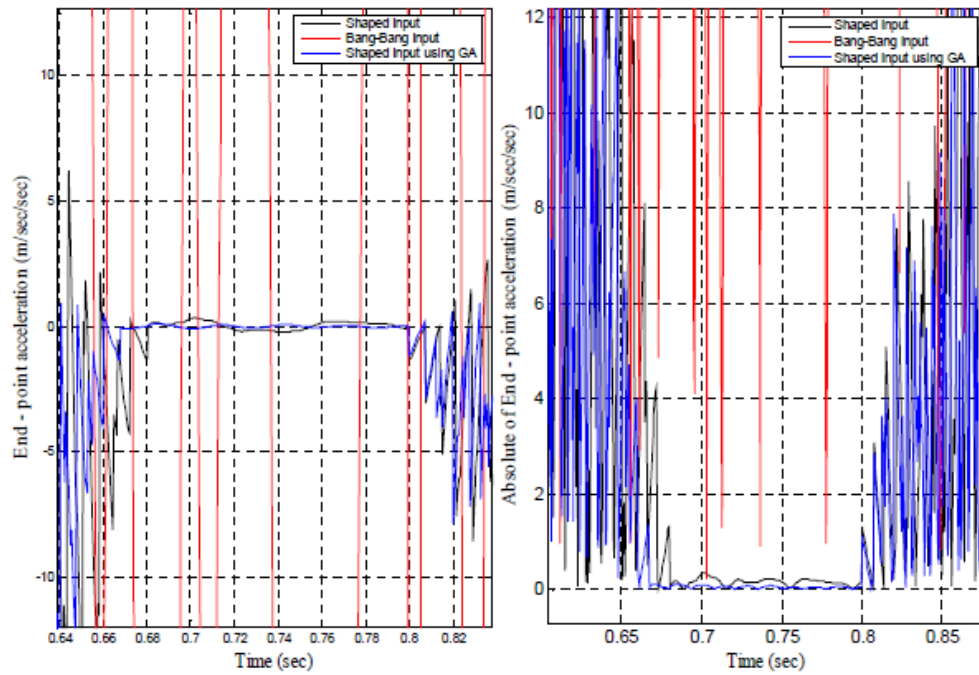


Figure13. End point acceleration (Enlarged in time domain).

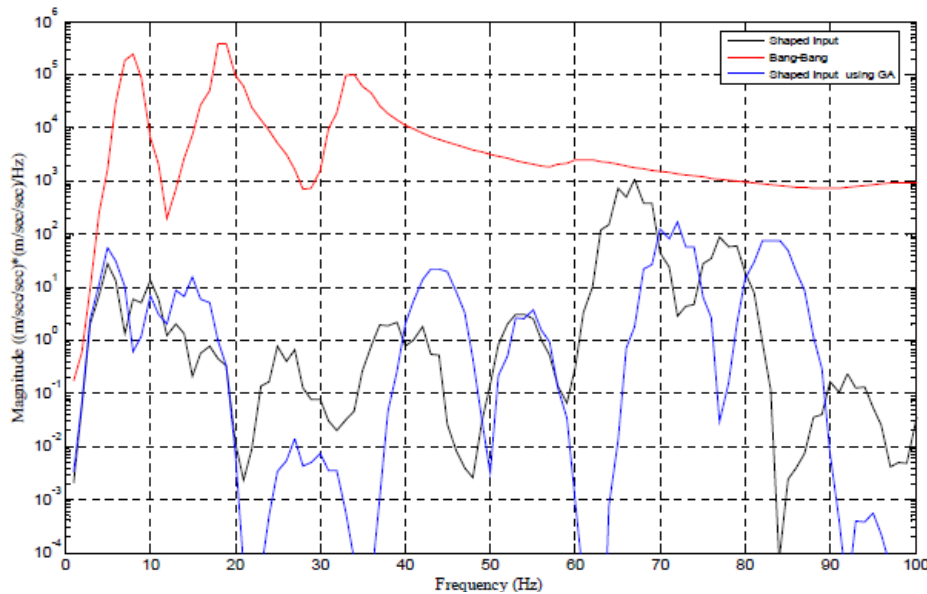


Figure13. End point acceleration (Spectrum density of end-point acceleration).

### 9. Conclusion

Flexible robot manipulator exhibits many advantages compared to their rigid counterparts. One of the major disadvantages of a flexible manipulator is the Presence of vibrations due its flexible nature. In this work, a single link flexible robot manipulator that moves in horizontal plane is considered. Modeling is done using FE method where the system is divided into 10 elements and the damping ratios of the system are deduced as 0.026, 0.038 and 0.040 for the first three vibration mode respectively to determine the amplitude of the impulse sequences. The vibrations in a system can be reduced using

input shaping techniques. This method is based on feed forward control strategy that requires simple estimated values of the natural frequencies and damping ratios. Input shaping is implemented by convolving a sequence of impulses with a desired system command to produce a shaped input. The robustness of natural frequencies error is increased proportionally to the number of impulse sequences. In this work, 4 impulses are considered to cancel one vibration mode, thus a total of 12 impulses are used. GA is used to further optimize the input shaping control technique by determining the optimal natural frequencies. The natural frequencies obtained from GA simulation for

0g payloads are 13.827039 Hz, 39.789425 Hz, and 65.872969 Hz for the first three vibration modes respectively. These values are used to determine the impulse sequences and it will be convolved with the bang-bang torque to produce shaped input that is then used to drive the system.

## References

- [1] Davis, L. (1987). Genetic Algorithm and Simulated Annealing.
- [2] Davis, L. (1991). Handbook of Genetic Algorithms.
- [3] De Jong, K. (1975). The Analysis and Behavior of a Class of Genetic Adaptive System.
- [4] Drapeau, V. and Wang, D. (1993). Verification of Closed-loop Shaped-input Controller for a five-bar-linkage Manipulator. IEEE International Conference on Robotic and Automation.
- [5] Farrenkopf, R. L. (1979). Optimal open-Loop Maneuver Profiles for Flexible Spacecraft. Journal of Guidance and Control, Nov.-Dec. 1979. 2(6): 491-498.
- [6] Goldberg, D. E. (1989). Genetic Algorithm in Search, Optimization and Machine Learning. Addison-Wesley.
- [7] Hollars, Micheal, G., Cannon and Robert, H., (1986). Experiments on the End-Point Control of a Flexible Two-Link Robot with Elastic Drives. AIAA, 86-97.
- [8] Junkins, J.L and Kim, Y. (1993). Introduction to Dynamics and Control of Flexible Structures. AIAA. Washington D.C.
- [9] Liu, Q. and Wie, B. (1992). Robust Time-Optimal Control of Uncertain Flexible Spacecraft. Journal of Guidance, Control and Dynamics. 15(3): 597-604.